Magnetic Resonance Imaging 57 (2019) 359–367

Contents lists available at ScienceDirect

Magnetic Resonance Imaging

journal homepage: www.elsevier.com/locate/mri

Original contribution

Dual-contrast pCASL using simultaneous gradient-echo/spin-echo multiband EPI

Ke Zhang[a,b], Volker J. Sturm[a], Lukas R. Buschle[a,b], Artur Hahn[a], Seong Dae Yun[c], N. Jon Shah[c,d], Martin Bendszus[a], Sabine Heiland[a], Heinz-Peter Schlemmer[b], Christian H. Ziener[a,b], Felix T. Kurz[a,b,*]

[a] Department of Neuroradiology, Heidelberg University Hospital, Heidelberg, Germany
[b] Department of Radiology, German Cancer Research Center, Heidelberg, Germany
[c] Institute of Neuroscience and Medicine 4, Medical Imaging Physics, Forschungszentrum Jülich, Germany,
[d] Department of Neurology, Faculty of Medicine, JARA, RWTH Aachen University, Aachen, Germany

ARTICLE INFO

Keywords:
Arterial spin labeling
Pseudo-continuous ASL
Multiband
Simultaneous multislice acquisition
Gradient-echo/spin-echo EPI

ABSTRACT

A 2D gradient-echo EPI is commonly employed for arterial spin labeling (ASL) readout to achieve fast whole brain coverage measurements. However, such a readout suffers from susceptibility artifacts induced by magnetic field inhomogeneities. To reduce these susceptibility effects, single–shot spin-echo EPI was proposed to be used for acquisitions in continuous ASL (CASL). To minimize functional and physiological variations, a gradient-echo (GE)/spin-echo (SE) dual-echo EPI readout of the CASL sequence is needed for a comparison between GE- and SE-based determination of cerebral blood flow (CBF). In this study, we employed a simultaneous GE/SE multiband EPI as the readout of a pseudo-CASL (pCASL) sequence. Motor cortex activations derived from a finger-tapping task and functional networks from resting state fMRI were compared for both GE and SE contrasts. Direct comparison of SE and GE contrasts revealed that GE ASL provides an improved sensitivity of functional activity in finger-tapping and in resting-state imaging. SE ASL, on the other hand, suffered less from susceptibility artifacts induced by magnetic field inhomogeneities and pulsatile flow artifacts.

1. Introduction

Cerebral blood flow (CBF) has been widely demonstrated to be coupled with brain function as well as brain metabolism [1], including during resting states [2–4]. Changes in CBF can be measured non-invasively with the method of arterial spin labeling (ASL) [5,6]. In ASL, the perfusion contrast in the images arises from the subtraction of two successively acquired images: one with, and one without a labeling of arterial spins after a small delay time. The subtracted signal is on the order of 1% of baseline signal, and the resting-state fluctuations cause only an additional fractional change [7]. The main challenges for using ASL to observe resting-state CBF fluctuations are the low signal-to-noise ratio (SNR), low temporal resolution, and possible contamination from blood oxygenation level dependent (BOLD) fluctuations [7]. Continuous ASL imaging, which provides higher SNR compared to pulsed ASL, has been used to investigate resting-state brain activities in relation to BOLD imaging [7–9]. High-pass filtering of the ASL signal allows for CBF oscillations to be isolated with reduced BOLD contamination [7]. Contamination of the perfusion estimate by BOLD can also be minimized by using either sinc subtraction or surround subtraction [10,11]. Connectivity maps from CBF and BOLD signals were demonstrated to be regionally similar [8,9,12,13].

A 2D gradient-echo (GE) EPI is commonly employed for ASL readout to achieve fast whole brain coverage measurements [14]. However, such a readout suffers from susceptibility artifacts induced by magnetic field inhomogeneities [14]. To reduce these susceptibility effects, spin-echo (SE) EPI was proposed to be used for acquisitions in perfusion fMRI [15]. The SE CASL technique was compared with a regular GE EPI sequence with the same slice thickness, as well as other imaging methods using thin slices and SE acquisitions. The results demonstrate improved functional sensitivity and efficiency of the SE CASL approach as compared with GE EPI techniques, and a trend of improved sensitivity as compared with the SE EPI approach in the brain regions affected by susceptibility artifacts. ASL images provide a robust alternative to BOLD methods for activation imaging in regions of high static field inhomogeneities [15]. To minimize functional and physiological variations, a simultaneous GE/SE EPI readout of the CASL sequence is needed for comparison.

* Corresponding author at: Department of Neuroradiology, Heidelberg University Hospital, 69120 Heidelberg, Germany.
E-mail address: felix.kurz@med.uni-heidelberg.de (F.T. Kurz).

https://doi.org/10.1016/j.mri.2018.11.018
Received 4 September 2018; Received in revised form 20 November 2018; Accepted 21 November 2018

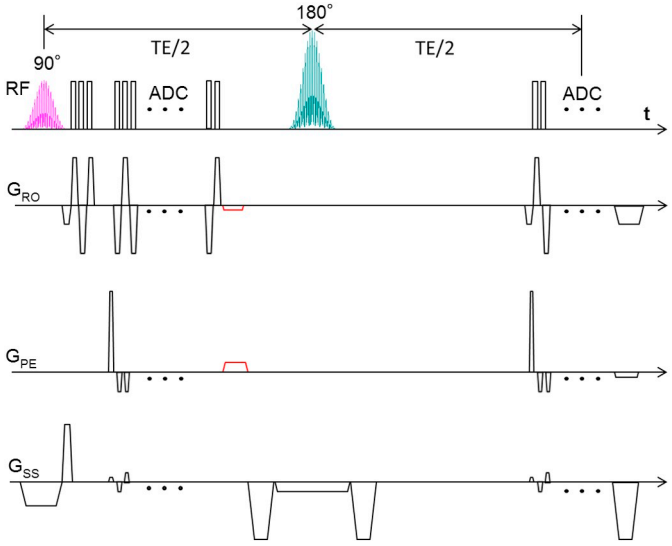

Fig. 1. Sequence diagram of the simultaneous GE/SE EPI sequence. Several slices are excited simultaneously using multiband RF pulse. An additional gradient blip scheme in slice direction with each phase encoding step shifts the slices in the PE direction and reduces the high g-factor penalties and effectively reduces the noise amplification in the reconstructed images. The rephasing gradient (in red) was inserted after GE readout to return the data acquisition to the k-space center. (For interpretation of the references to colour in this figure legend, the reader is referred to the web version of this article.)

We make further use of the multiband EPI method in ASL, a recently proposed technique to improve the temporal resolution and efficiency of ASL data acquisition to eventually obtain high-resolution images of the whole brain, see e.g. [16] and references therein. While multiband ASL has been developed for single shot and multi time-point ASL to increase SNR to achieve a more accurate CBF estimation [17–21], we here adapt it for a dual GE/SE multiband EPI-based pCASL readout to allow for a simultaneous comparison of two whole brain perfusion images. The phases imprinted by the first EPI readout are thereby canceled by the rephasing gradients just before the refocusing pulse to easily enable in-plane partial Fourier imaging (Fig. 1). Motor cortex activations derived from a finger-tapping task were compared for both GE and SE contrasts. Whole brain quantitative cerebral blood flow maps and resting state networks were compared.

2. Methods

16 healthy young volunteers (8 male, 8 female) were scanned using a 64-channel head receive radiofrequency (RF) coil on a 3T Prisma Siemens scanner (Siemens Healthcare, Erlangen, Germany). Written and informed consent was obtained from all subjects and the study was approved by the Ethics Committee of the Medicine Faculty of Heidelberg University Hospital. The study was conducted according to the Declaration of Helsinki.

Table 1
Correlation coefficients between GE and SE CBF signal time courses in different networks for each subject.

Sub.	Sensorimotor	Auditory	Primary visual	Higher visual	Default-mode	Salience	Left ECN	Right ECN
1	0,22	−0,18	0,42	0,56	0,31	0,53	0,73	0,21
2	0,08	0,29	0,29	0,77	0,35	0,29	0,68	0,30
3	0,69	0,44	0,68	0,67	0,39	0,44	0,64	0,48
4	0,64	0,47	0,66	0,75	0,41	0,49	0,47	0,48
5	0,57	0,34	0,48	0,84	0,64	0,31	0,85	0,42
6	0,52	0,27	0,51	0,84	0,45	0,59	0,70	0,65
7	0,59	0,56	0,53	0,76	0,47	0,55	0,69	0,79
8	0,12	0,23	0,47	0,83	0,29	0,11	0,79	0,46
9	0,01	0,35	0,52	0,65	0,59	0,77	0,70	0,65
10	0,66	0,55	0,70	0,45	0,50	0,47	0,48	0,55
11	0,61	0,62	0,67	0,50	0,44	0,44	0,70	0,55
12	0,67	0,64	0,60	0,63	0,43	0,71	0,03	−0,34
13	0,89	0,49	0,70	0,77	0,50	0,38	0,71	0,61
14	0,43	0,38	−0,01	0,41	0,21	0,26	0,58	0,62
15	0,23	0,16	0,51	0,40	0,34	0,26	0,53	0,40
16	0,55	0,22	0,52	0,82	0,44	0,55	0,68	0,49

Table 2
P-values of the correlations between GE and SE CBF signal time courses in different networks for each subject. If p-values are < 0.001, the correlation is highly significant.

Sub.	Sensorimotor	Auditory	Primary visual	Higher visual	Default-mode	Salience	Left ECN	Right ECN
1	0,014	0,045	0,000	0,000	0,000	0,000	0,000	0,017
2	0,379	0,001	0,001	0,000	0,000	0,001	0,000	0,001
3	0,000	0,000	0,000	0,000	0,000	0,000	0,000	0,000
4	0,000	0,000	0,000	0,000	0,000	0,000	0,000	0,000
5	0,000	0,000	0,000	0,000	0,000	0,000	0,000	0,000
6	0,000	0,002	0,000	0,000	0,000	0,000	0,000	0,000
7	0,000	0,000	0,000	0,000	0,000	0,000	0,000	0,000
8	0,158	0,009	0,000	0,000	0,001	0,204	0,000	0,000
9	0,912	0,000	0,000	0,000	0,000	0,000	0,000	0,000
10	0,000	0,000	0,000	0,000	0,000	0,000	0,000	0,000
11	0,000	0,000	0,000	0,000	0,000	0,000	0,000	0,000
12	0,000	0,000	0,000	0,000	0,000	0,000	0,777	0,000
13	0,000	0,000	0,000	0,000	0,000	0,000	0,000	0,000
14	0,000	0,000	0,924	0,000	0,017	0,002	0,000	0,000
15	0,010	0,066	0,000	0,000	0,000	0,003	0,000	0,000
16	0,000	0,013	0,000	0,000	0,000	0,000	0,000	0,000

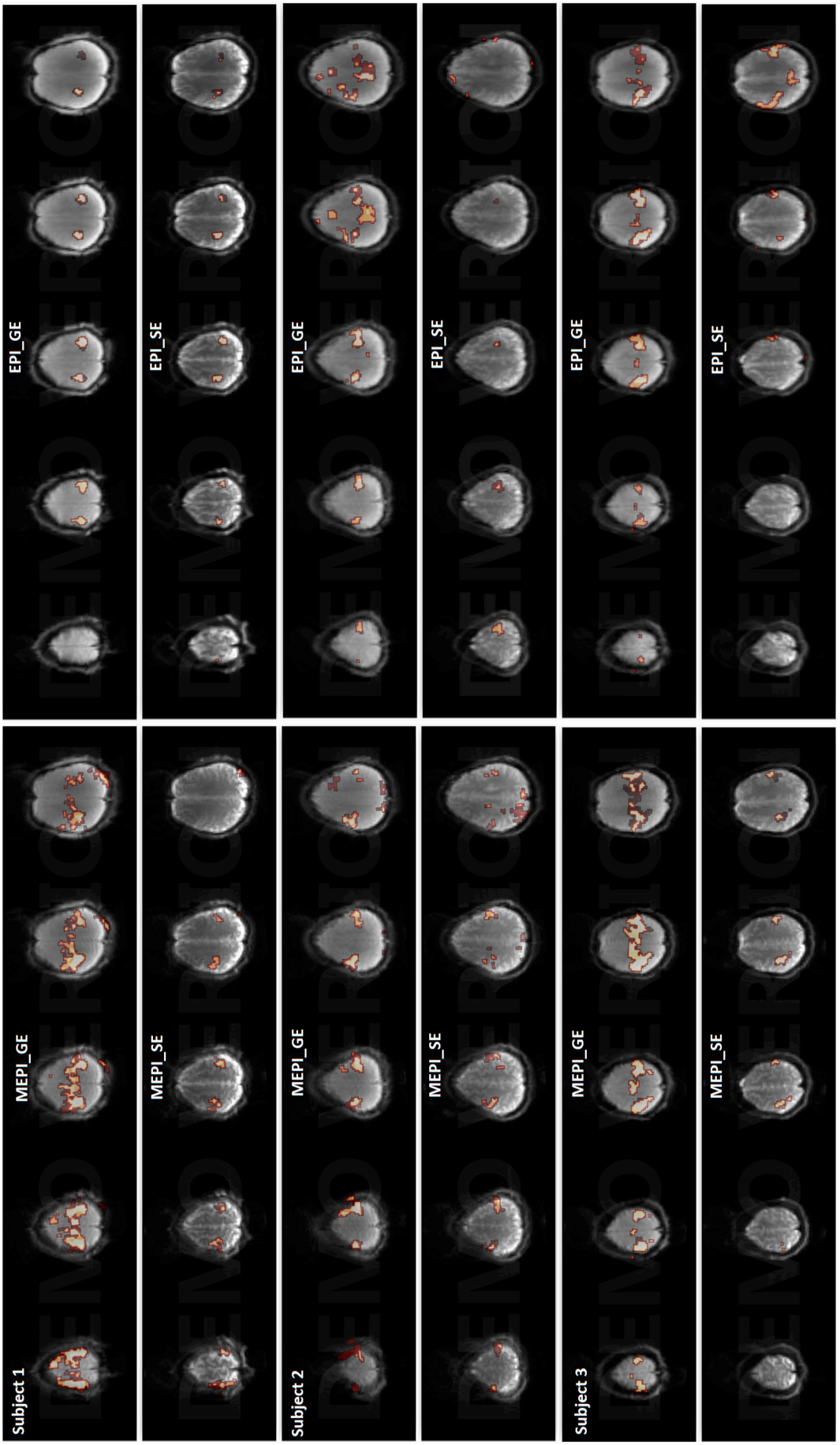

Fig. 2. Brain activities from a finger-tapping task detected by the multi-band EPI (MEPI) and single-band EPI pCASL sequence. The activity region was taken at a threshold of $p < 0.001$.

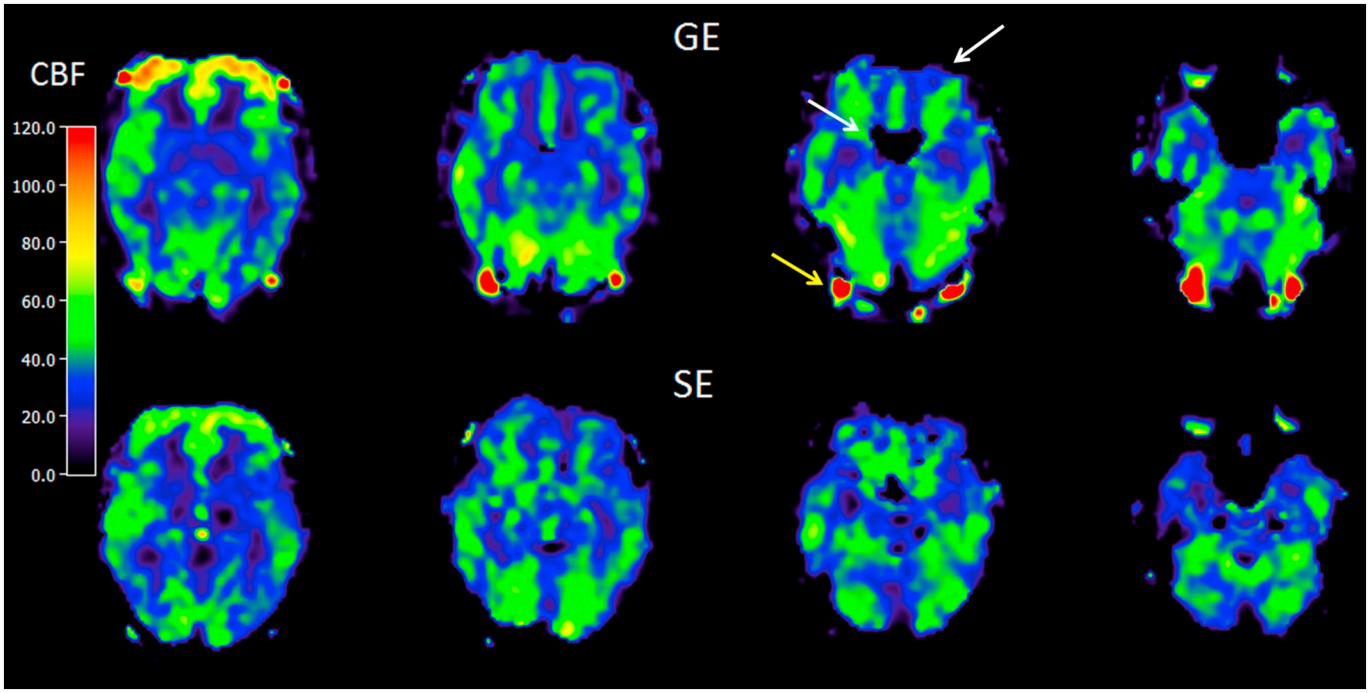

Fig. 3. CBF maps acquired by simultaneous GE/SE EPI readouts. Both GE and SE CBF maps are shown in the range of 0–120 mL/100 g/min. GE ASL maps showed increased susceptibility artifacts at the region of frontobasal cerebrumand frontal lobe (white arrows), and increased pulsatile flow artifacts from superficial cranial arteries around the brain (yellow arrow), when compared to SE ASL. (For interpretation of the references to colour in this figure legend, the reader is referred to the web version of this article.)

2.1. Finger-tapping

For block-designed finger-tapping tasks, 88 measurements with 44 pairs of label-control volumes were obtained, which include five and a half tapping/rest cycles with 16 measurements (8 pairs) per cycle and 8 measurements (4 pairs) per half cycle. Sequence parameters for the multiband EPI sequence were taken as follows: TE (GE/SE) = 14.5/78 ms, dim = 64 × 64 × 20, multiband factor = 2, partial Fourier = 6/8, resolution = 3.4 × 3.4 × 5 mm^3, time of labeling = 1.4 s, PLD = 1 s, TR = 3.55 s. Here 10 multiband excitations in EPI were performed which yields full 20 slices. For comparison, we imaged with a single-band EPI sequence consisting of 10 slices, which were placed at the same location of the motor cortex as the multi-band EPI sequence slices. The total measurement time for the finger-tapping task acquisitions was 5.2 min. CBF was calculated after preprocessing with realignment, reslicing and smoothing algorithms in Matlab (R2015a, The MathWorks, Natick, MA, USA). Calculation of CBF was obtained based on the surround subtraction method [10,11]. Two sample *t*-tests were used to compare the CBF time series between on and off states of finger-tapping tasks.

2.2. Resting-state

For resting-state measurements, 130 measurements were acquired with the same parameters as for the finger-tapping task. The total measurement time for resting-state acquisitions was 7:45 min. The resting-state ASL was preprocessed using DPARSF (http://rfmri.org/DPARSF) with the following steps: motion correction, spatial normalization to the standard Montreal Neurological Institute (MNI) space, smoothing along three directions with FWHM = 6 mm, temporal filtering (0.07–0.14 Hz), CBF calculation, detrending, regressing out certain nuisance covariates, including 6 head motion parameters, global mean signal, white matter signal and cerebrospinal fluid signal. The functional images were normalized to MNI space by using unified segmentations on the T1-weighted images of the same patient to improve the accuracy of spatial normalization. This process contained three steps: coregistration, segmentation and writing normalization parameters. To ensure that CBF values were not contaminated by the BOLD signal, spatially smoothed ASL raw data was split into a high-pass filtered series with a cut-off of 1/(4*TR) [7], corresponding to 0.07 Hz in our case, and a low-pass series obtained as the residuals of the filtering. The high-pass filtering range applied to the ASL signal, to generate uncontaminated CBF fluctuations, was 0.07–0.14 Hz. The high-passed filtered series was used to obtain the CBF signal, while the low-pass filtered series contained the EPI-BOLD signal [7]. Calculation of CBF was obtained using ASLtbx [22] and the surround subtraction method on the high-pass filtered series [10,11]. After CBF calculation, CBF data were detrended and nuisance covariates were regressed out.

Finally, a conventional 3D MP-RAGE sequence of 6 min was performed to acquire T1-weighted anatomical images (resolution = 1 mm^3 isotropic, TE/TR = 4.45/20 ms, flip angle = 25°, 256 × 256 × 192, GRAPPA factor = 2).

2.3. Seed-based functional connectivity analyses

To obtain the corresponding networks in the resting-state, 8 seed ROIs were placed in the left precentral gyrus (Talairach coordinates: −53, −7, 29) for the sensorimotor network, left transverse temporal gyrus (−50, −21, 11) for the auditory network, left cuneus (BA 17: −6, −76, 11) for the primary visual network, left inferior occipital gyrus (BA17: −20, −94, −8) for the higher visual network, left posterior cingulate cortex (−12, −54, 10) for the default-mode network, left dorsal cingulate cortex (−4, 26, 34) for the salience network, left inferior parietal cortex (−48, −63, 38) for the left executive-control network (ECN), and right inferior parietal cortex (45, −58, 42) for the right ECN. The average time course of each seed ROI was extracted as a reference time course to calculate the cross-correlation coefficient (cc) map for each individual which was then transformed to z-value maps with Fisher's z transform. A one-sample *t*-test was performed on the z-value maps to obtain significant functional connectivity maps at a

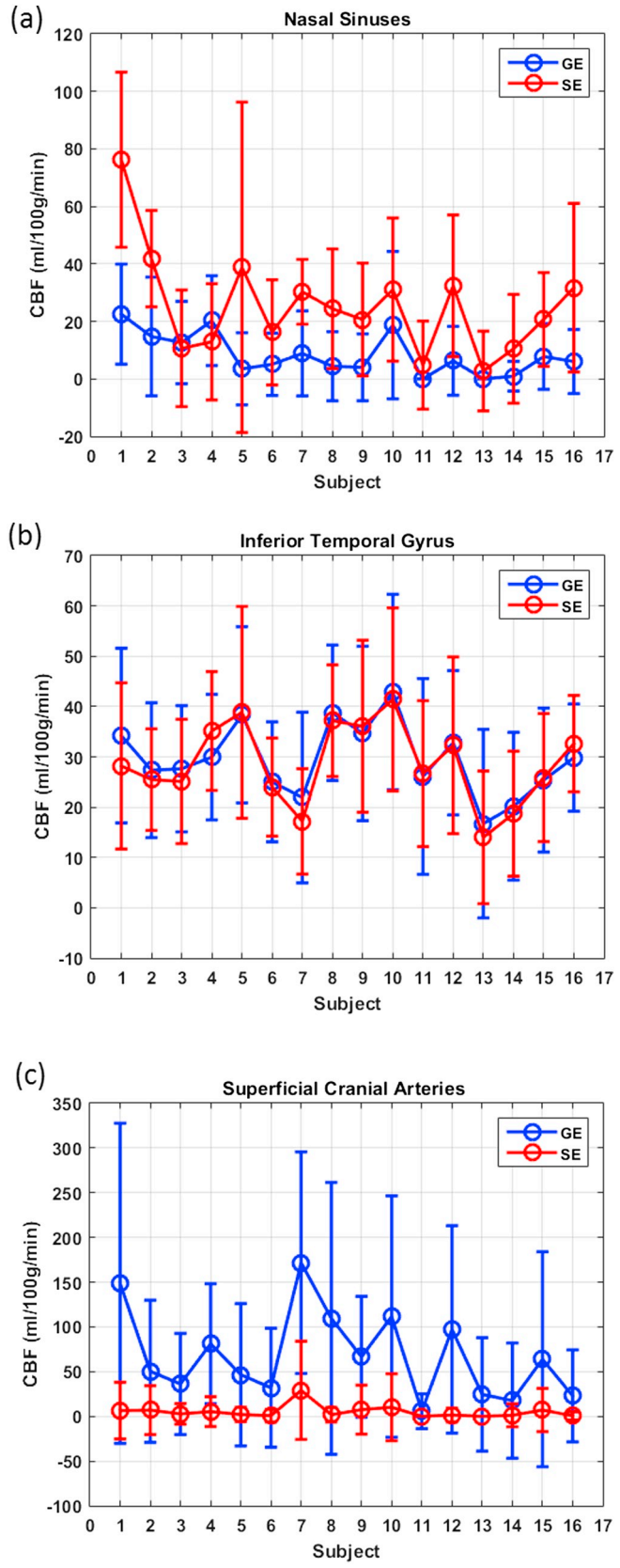

Fig. 4. (a) GE and SE CBF of a ROI defined at the region of the nasal sinuses, based on an averaged map from all subjects. (b) GE and SE CBF of a ROI defined at the region of the inferior temporal gyrus. (c) GE and SE CBF of a ROI defined at the region of the superficial cranial arteries. Mean values are marked with circles and standard deviations are shown as error bars.

group level, which were thresholded at $t > 7$ with a cluster size resulting in p-value at $p < 0.05$ (FWE).

Since a simultaneous GE/SE dual-echo EPI sequence was utilized, the GE and SE signal are expected to be highly correlated. To calculate the correlations between GE and SE CBF signals, time courses of 8 networks were extracted for each subject. The correlation coefficients are listed in Table 1 and the p-values of the correlations are shown in Table 2.

3. Results

The individual activation maps after finger-tapping were superimposed upon GE and SE images with a threshold of $p < 0.001$, see Fig. 2. Both the perfusion data from GE and the SE EPI scan yielded robust activation at the region of the motor cortex. The perfusion data acquired by GE EPI showed more activation than the perfusion data acquired by SE EPI.

In Fig. 3 we show the quantitative CBF map of a representative subject, based on both the GE and SE EPI readout, respectively. The CBF values from both readouts were in the range of 0–120 mL/100 g/min. The CBF maps exhibited similar contrast, though the SE CBF maps appeared less distorted at the tissue-air interface regions such as region at frontobasal cerebrum, frontal lobe and temporal lobe. Signal voids in the same regions were clearly smaller in the SE CBF maps. Also, we observed a decrease in pulsatile flow artifacts from superficial cranial arteries around the brain in SE readouts.

To quantify the effect of magnetic field inhomogeneity on image quality, we compared mean CBF from a representative ROI in the frontobasal cerebrum, defined on an averaged GE CBF map from all subjects. A ROI at the inferior temporal gyrus was defined based on the respective averaged Anatomical Automatic Labeling (AAL) map [23]. For the region of the frontlbasal cerebrum, we found that mean CBF signals from the ROI in GE CBF maps were mostly lower compared to SE CBF maps for the same ROI, due to the increased number of signal voids, see Fig. 4(a). In contrast, mean CBF in ROIs on the inferior temporal gyrus were similar in GE and SE CBF maps, see Fig. 4(b). To compare the pulsatile flow artifacts, a ROI in the region of the superficial cranial arteries was manually defined based on an averaged GE CBF map from all 16 subjects. We found decreased CBF in this region in SE CBF compared to GE CBF, see Fig. 4(c).

For comparison, the seed-based functional networks generated from GE and SE ASL are displayed in Fig. 5. 8 resting-state functional networks were generated, including the sensorimotor network, auditory network, primary visual network, higher visual network, default-mode network, salience network, left ECN, and right ECN. The perfusion data acquired by GE EPI showed greater activation than that acquired by SE EPI: the numbers of active voxels with a t value greater 7 in GE and SE ASL network maps, as well as the summed t of these active voxels, are presented in Fig. 6(a) and (b), respectively. It can be seen that, in all networks, GE ASL has the higher active voxel count and summed t when compared to SE ASL.

Time courses of GE (1st echo) and SE (2nd echo) CBF signals in the default-node network (a) and primary visual cortex (b) of a single subject are shown in Fig. 7. The correlation coefficients between GE and SE signals are 0.44 ($p < 0.001$) and 0.67 ($p < 0.001$) in the default-node network and primary visual cortex, respectively. As expected, the correlations between GE and SE CBF signals are high (Tables 1 and 2) with most of the p-values below 0.0001.

4. Discussion

In this work, a dual GE/SE multiband EPI was developed as a pCASL readout, to allow for a simultaneous comparison of two whole brain perfusion images. With a multiband factor of 2, the optimized GE/SE EPI sequence achieves twice the number of slices while maintaining the same repetition time as the SB technique. By inserting the rephasing

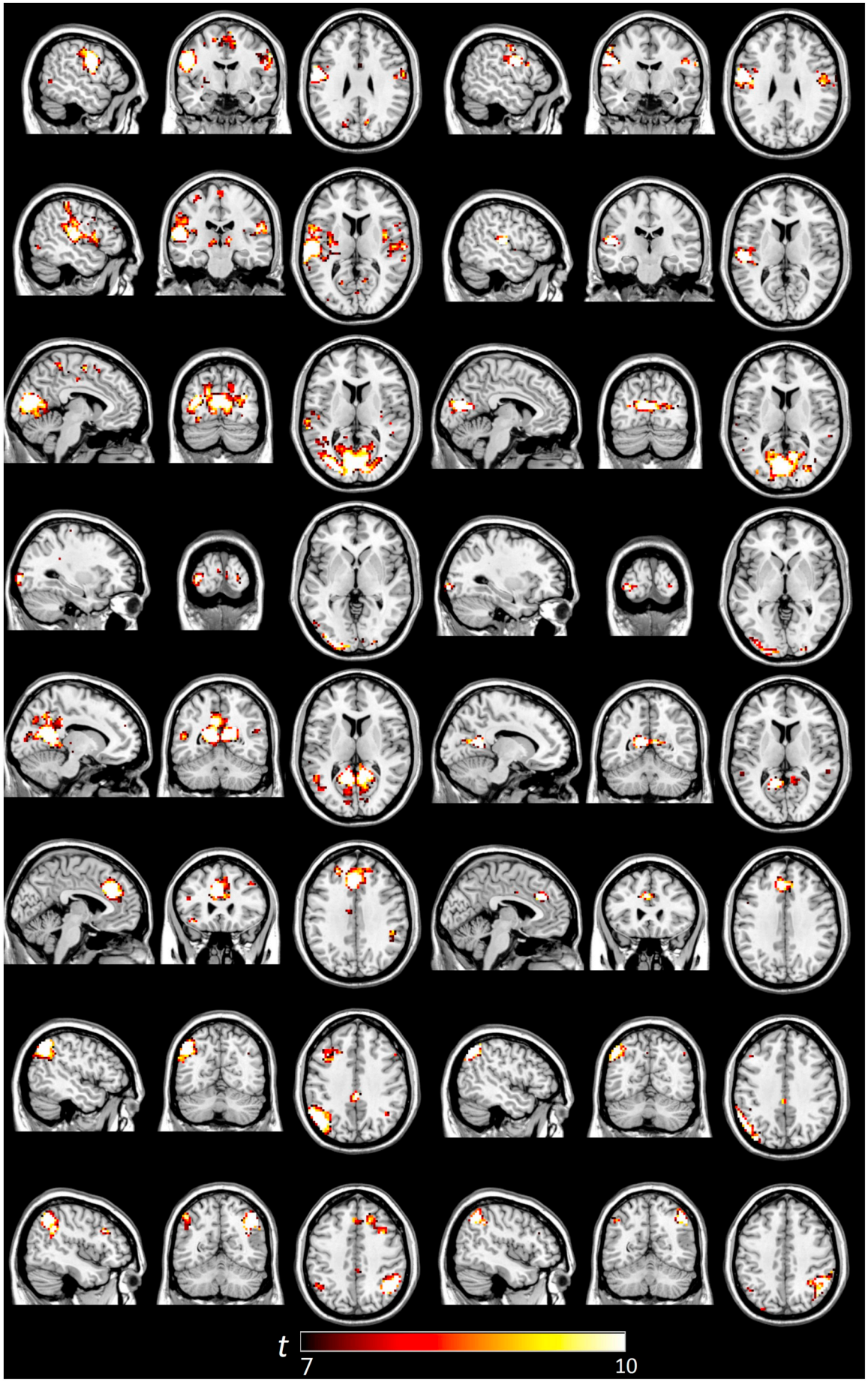

(caption on next page)

Fig. 5. Brain networks detected by the seed-based analysis of the GE (left) and SE (right) contrast, including sensorimotor, auditory, primary visual, higher visual, default mode, salience and left, right executive control networks.

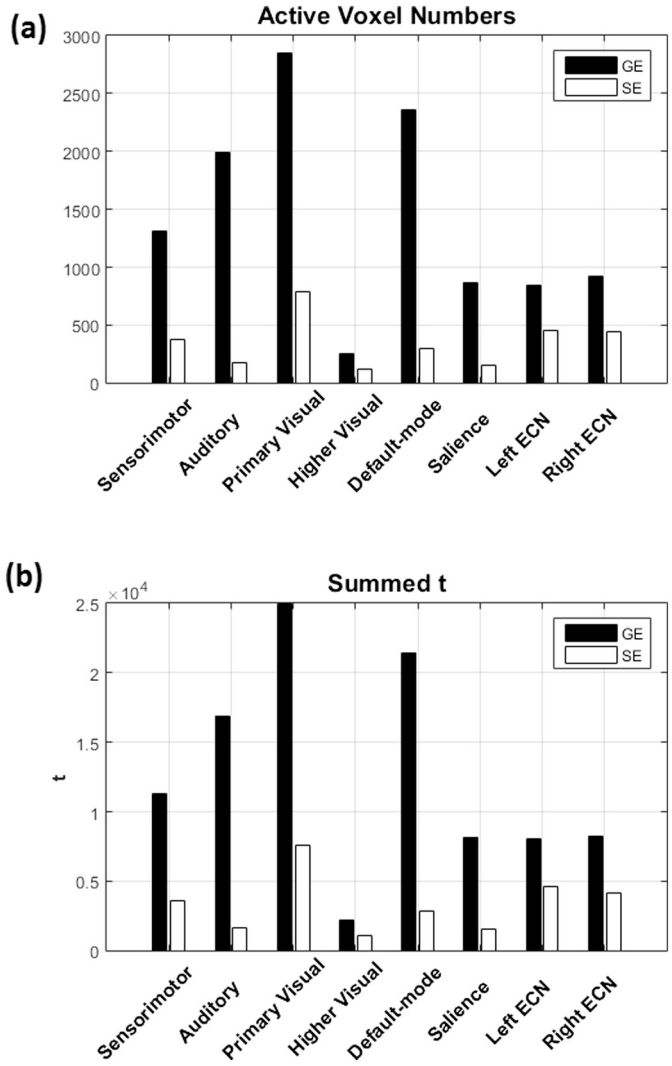

Fig. 6. (a) Active voxels with t values > 7 in typical GE and SE ASL networks. (b) Summed t of these active voxels in the same networks.

gradient after GE EPI (Fig. 1), partial Fourier imaging can be easily achieved. Without the rephasing gradient, the actual position in k-space is flipped to the diagonal position of the k-space after application of a 180° pulse. However by using partial Fourier acceleration, the start point and end point in k-space are not point-symmetric to the k-space center, so that the k-space position before the second EPI read out train, which depends on the acceleration factor, needs to be corrected. To ensure correct data acquisition, and to allow the usage of a standard EPI module, the phases produced by the EPI readout were canceled just before the refocusing pulse.

We subsequently acquired quantitative CBF maps using a 2D EPI based pCASL sequence. High perfusion sensitivity was achieved using a long labeling pulse, and surround subtraction was used to achieve a high temporal resolution and to avoid contamination of BOLD signals. We also added high-pass filtering into CBF post-processing to suppress BOLD fluctuations.

According to the number of active voxels and summed t at the region t > 7, GE ASL showed higher values in all networks when compared to SE ASL (Fig. 6), suggesting that, in these networks, GE ASL provides a better sensitivity of functional activity in the resting-state than SE ASL. In comparison with the GE readout, SE active regions were more confined (Figs. 2, 5 and 6), partially due to reduced contributions from large vessels [24]. SE signal sensitivity is significantly reduced due to refocusing of the dephasing effect around large vessels compared to the GE readout [25]. GE BOLD sensitivity for functional connectivity is larger with respect to SE BOLD, as demonstrated in prior studies [26,27]. T_2-weighted SE sequences have been proposed as a promising alternative when an increased functional localization to the capillary bed is desired, because static dephasing effects around larger vessels are refocused by the 180° radiofrequency pulse [28], therefore trading sensitivity for a higher spatial specificity for microvasculature [29]. In addition, the improved sensitivity of functional activity in the resting-state GE ASL, when compared to SE ASL, may result from a higher SNR in the GE readout, presumably due to the fact that SE was acquired at a longer TE and only partial k-space sampling [30]. SE CBF maps also suffered considerably less from susceptibility artifacts in air-tissue regions such as the region at frontobasal cerebrum, frontal and temporal lobe (Figs. 3 and 4(a)), in agreement with the literature [15]. In brain regions affected by macroscopic magnetic field inhomogeneities, the BOLD sensitivity in SE EPI may be considerably higher compared to GE EPI. For example, when using SE EPI, additional frontopolar and ventral frontomedian activations were observed during a Stroop colour–word matching task, which could not be detected using GE EPI [31]. Similar results were reported in the hippocampus during a hyperventilation task [32] and in the inferior temporal lobes during a semantic categorization task [33]. SE EPI may therefore provide an interesting alternative for fMRI in regions affected by macroscopic magnetic field inhomogeneities [26,34,35].

We also observed that the SE readout was less prone to pulsatility artifacts in large vessels (Figs. 3 and 4(c)), likely due to the fact that the slice-selective 180° pulses after an initial 90° pulse do not refocus rapidly flowing spins and therefore create a signal void where signal artifacts would occur during GE readout [27]. Another possibility could be that the crusher gradients around the refocusing pulse serve as weak flow nulling. However, with the parameters used in the sequence it can be easily verified that, the second effect is negligible.

To compare the time courses of GE and SE CBF signals, correlation coefficients and p-values of the correlations were calculated in different networks for each subject (Tables 1 and 2). Most of the p-values were below 0.001, which indicates the correlations were highly significant.

One caveat of this study is a relatively short PLD (1 s) in the pCASL sequence to assess the resting-state activities. A short PLD underestimates the perfusion in regions with long blood arrival time such as white matter [36]. A longer PLD can ensure that the majority of the voxels are filled with blood; however, it also leads to a decreased SNR due to signal decay. Higher SNR and temporal resolution due to short PLD increase the sensitivity of ASL in detecting the resting state networks.

In conclusion, a dual-contrast pCASL sequence using simultaneous GE/SE multiband EPI readout was implemented to investigate the nature and differences between SE and GE CBF. Motor cortex activations derived from a finger-tapping task were compared for both GE and SE contrasts. Whole brain covered quantitative cerebral blood flow (CBF) and resting state networks were compared. After direct

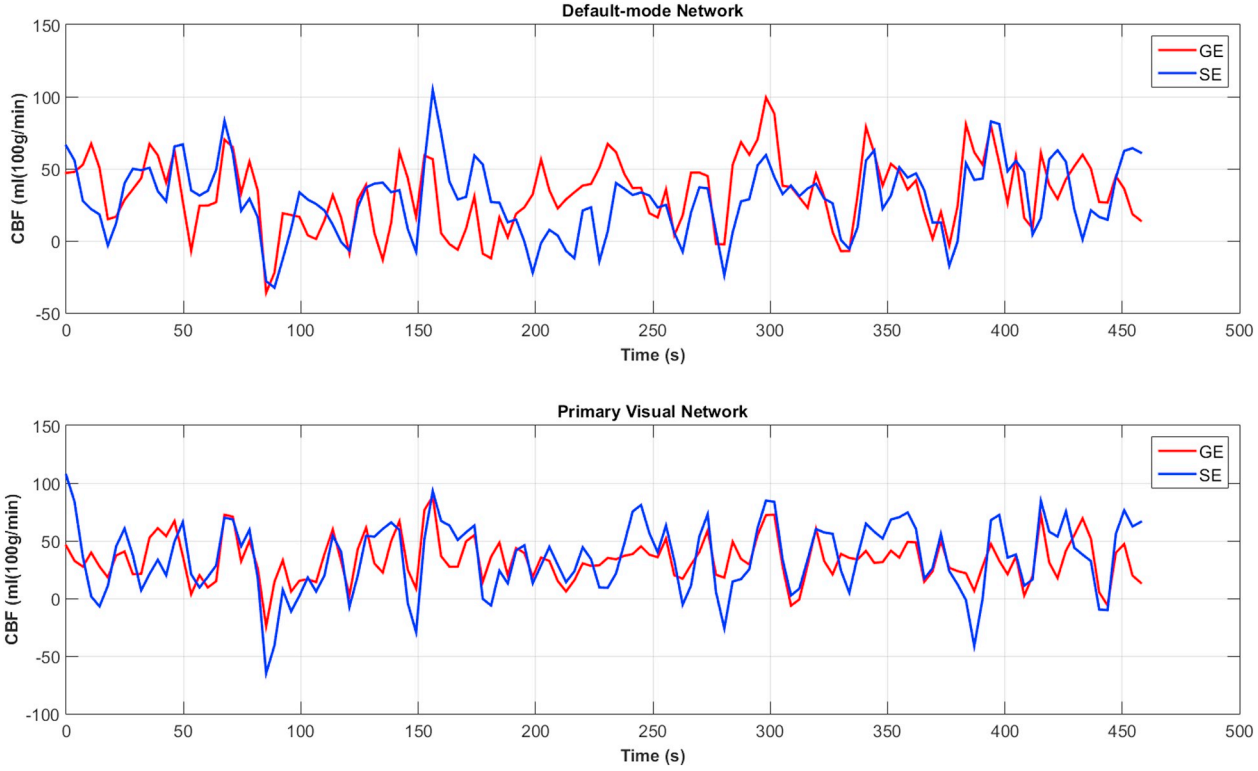

Fig. 7. Time course of GE and SE CBF signals in the default-node network (a) and primary visual cortex (b) of a single subject.

comparison of SE and GE contrasts, we found that GE ASL provides a better sensitivity of functional activity in the finger-tapping task and in resting-state imaging. From quantitative CBF maps acquired by both readouts, we further observed that SE ASL suffered less from susceptibility artifacts induced by magnetic field inhomogeneities and pulsatile flow artifacts than GE ASL.

References

[1] Raichle ME. Behind the scenes of functional brain imaging: a historical and physiological perspective. Proc Natl Acad Sci U S A 1998;95(3):765–72.
[2] Fox PT, Raichle ME. Focal physiological uncoupling of cerebral blood flow and oxidative metabolism during somatosensory stimulation in human subjects. Proc Natl Acad Sci U S A 1986;83(4):1140–4.
[3] Fox PT, Raichle ME, Mintun MA, Dence C. Nonoxidative glucose consumption during focal physiologic neural activity. Science 1988;241(4864):462–4.
[4] Raichle ME, MacLeod AM, Snyder AZ, Powers WJ, Gusnard DA, Shulman GL. A default mode of brain function. Proc Natl Acad Sci U S A 2001;98(2):676–82.
[5] Barbier EL, Lamalle L, Decorps M. Methodology of brain perfusion imaging. J Magn Reson Imaging 2001;13(4):496–520.
[6] Golay X, Hendrikse J, Lim TC. Perfusion imaging using arterial spin labeling. Top Magn Reson Imaging 2004;15:10–27.
[7] Chuang KH, Van Gelderen P, Merkle H, Bodurka J, Ikonomidou VN, Koretsky AP, et al. Mapping resting-state functional connectivity using perfusion MRI. Neuroimage 2008;40(4):1595–605.
[8] Viviani R, Messina I, Walter M. Resting state functional connectivity in perfusion imaging: correlation maps with BOLD connectivity and resting state perfusion. Plos One 2011;6(11).
[9] Li ZJ, Zhu YS, Childress AR, Detre JA, Wang Z. Relations between BOLD fMRI-derived resting brain activity and cerebral blood flow. Plos One 2012;7(9).
[10] Liu TT, Wong EC. A signal processing model for arterial spin labeling functional MRI. Neuroimage 2005;24(1):207–15.
[11] Lu HZ, Donahue MJ, van Zijl PCM. Detrimental effects of BOLD signal in arterial spin labeling fMRI at high field strength. Magn Reson Med 2006;56(3):546–52.
[12] Chen JJ, Jann K, Wang DJ. Characterizing resting-state brain function using arterial spin labeling. Brain Connect 2015;5(9):527–42.
[13] Fukunaga M, Horovitz SG, de Zwart JA, van Gelderen P, Balkin TJ, Braun AR, et al. Metabolic origin of BOLD signal fluctuations in the absence of stimuli. J Cereb Blood Flow Metab 2008;28(7):1377–87.
[14] Wolf RL, Detre JA. Clinical neuroimaging using arterial spin-labeled perfusion magnetic resonance imaging. Neurotherapeutics 2007;4(3):346–59.
[15] Wang JJ, Li L, Roc AC, Alsop DC, Tang K, Butler NS, et al. Reduced susceptibility effects in perfusion fMRI with single-shot spin-echo EPI acquisitions at 1.5 tesla. Magn Reson Imaging 2004;22(1):1–7.
[16] van Osch MJ, Teeuwisse WM, Chen Z, Suzuki Y, Helle M, Schmid S. Advances in arterial spin labelling MRI methods for measuring perfusion and collateral flow. J Cereb Blood Flow Metab 2018;38(9):1461–80.
[17] Feinberg DA, Beckett A, Chen L. Arterial spin labeling with simultaneous multi-slice echo planar imaging. Magn Reson Med 2013;70(6):1500–6.
[18] Kim T, Shin WY, Zhao TJ, Beall EB, Lowe MJ, Bae KT. Whole brain perfusion measurements using arterial spin labeling with multiband acquisition. Magn Reson Med 2013;70(6):1653–61.
[19] Wang Y, Moeller S, Li XF, Vu AT, Krasileva K, Ugurbil K, et al. Simultaneous multi-slice turbo-FLASH imaging with CAIPIRINHA for whole brain distortion-free pseudo-continuous arterial spin labeling at 3 and 7 T. Neuroimage 2015;113:279–88.
[20] Zhang K, Yun SD, Shah NJ. Tripled readout slices in multi time-point pCASL using multiband look-locker EPI. Plos One 2015;10(11).
[21] Li X, Wang D, Auerbach EJ, Moeller S, Ugurbil K, Metzger GJ. Theoretical and experimental evaluation of multi-band EPI for high-resolution whole brain pCASL imaging. Neuroimage 2015;106:170–81.
[22] Wang Z, Aguirre GK, Rao H, Wang J, Fernandez-Seara MA, Childress AR, et al. Empirical optimization of ASL data analysis using an ASL data processing toolbox: ASLtbx. Magn Reson Imaging 2008;26(2):261–9.
[23] Tzourio-Mazoyer N, Landeau B, Papathanassiou D, Crivello F, Etard O, Delcroix N, et al. Automated anatomical labeling of activations in SPM using a macroscopic anatomical parcellation of the MNI MRI single-subject brain. Neuroimage 2002;15(1):273–89.
[24] Kim SG, Ogawa S. Biophysical and physiological origins of blood oxygenation level-dependent fMRI signals. J Cereb Blood Flow Metab 2012;32(7):1188–206.
[25] Ziener CH, Kampf T, Reents G, Schlemmer HP, Bauer WR. Spin dephasing in a magnetic dipole field. Phys Rev E 2012;85(5).
[26] Chiacchiaretta P, Ferretti A. Resting state BOLD functional connectivity at 3T: spin Echo versus gradient Echo EPI. Plos One 2015;10(3).
[27] Bandettini PA, Wong EC, Jesmanowicz A, Hinks RS, Hyde JS. Spin-Echo and Gradient-Echo epi of human brain activation using BOLD contrast - a comparative-study at 1.5 T. NMR Biomed 1994;7(1–2):12–20.
[28] Ziener CH, Kampf T, Melkus G, Jakob PM, Schlemmer HP, Bauer WR. Signal evolution in the local magnetic field of a capillary – analogy to the damped driven harmonic oscillator. Magn Reson Imaging 2012;30(4):540–53.
[29] Norris DG. Spin-echo fMRI: the poor relation? Neuroimage 2012;62(2):1109–15.
[30] Rua C, Costagli M, Symms MR, Biagi L, Donatelli G, Cosottini M, et al. Characterization of high-resolution gradient Echo and Spin Echo EPI for fMRI in the human visual cortex at 7 T. Magn Reson Imaging 2017;40:98–108.
[31] Norris DG, Zysset S, Mildner T, Wiggins CJ. An investigation of the value of spin-echo-based fMRI using a Stroop color-word matching task and EPI at 3 T. Neuroimage 2002;15(3):719–26.
[32] Naganawa S, Norris DG, Zysset S, Mildner T. Regional differences of fMR signal changes induced by hyperventilation: comparison between SE-EPI and GE-EPI at 3-

T. J Magn Reson Imaging 2002;15(1):23–30.
[33] Schwarzbauer C, Raposo A, Tyler LK. Spin-echo fMRI overcomes susceptibility-induced signal losses in the inferior temporal lobes. Human brain mapping. 2006. p. 233. Florence, Italy.
[34] Khatamian YB, Golestani AM, Ragot DM, Chen JJ. Spin-Echo resting-state functional connectivity in high-susceptibility regions: accuracy, reliability, and the impact of physiological noise. Brain Connect 2016;6(4):283–97.
[35] Schwarzbauer C, Mildner T, Heinke W, Brett M, Deichmann R. Dual echo EPI–the method of choice for fMRI in the presence of magnetic field inhomogeneities? Neuroimage 2010;49(1):316–26.
[36] Zhang K, Herzog H, Mauler J, Filss C, Okell TW, Kops ER, et al. Comparison of cerebral blood flow acquired by simultaneous [O-15]water positron emission tomography and arterial spin labeling magnetic resonance imaging. J Cereb Blood Flow Metab 2014;34(8):1373–80.